 doi:10.20944/preprints202012.0276.v1

*Article*

# *Operando* in-SEM study of micro-deformation and fracture behaviour of carbonized elastomer-based composites

**Eugene S. Statnik [1,*], Semen D. Ignatyev [2], Andrey A. Stepashkin [2], Alexey I. Salimon [1,2], Dilyus Chukov [2], Sergey D. Kaloshkin [2], and Alexander M. Korsunsky [3,1]**

[1] HSM lab, Center for Energy Science and Technology, Skoltech, Moscow 121205, Russia; a.salimon@skoltech.ru (A.I.S.)
[2] Center for Composite Materials, NUST MISiS, Moscow 119049, Russia; ignatyev.s.11@gmail.com (S.D.I), a.stepashkin@misis.ru (A.A.S.), dil_chukov@mail.ru (D.Ch.), kaloshkin@misis.ru (S.D.K.)
[3] MBLEM, Department of Engineering Science, University of Oxford, Oxford OX1 3PJ, UK; alexander.korsunsky@eng.ox.ac.uk (A.M.K.)
* Correspondence: eugene.statnik@skoltech.ru (E.S.S.)

**Highlights:**

- *In situ* loading with DIC allows strain mapping in the complex-shaped sample(s), and matching FEA simulation to it allows reliable determination of Young's modulus.
- Carbonization leads to a two-fold increase of strength, and considerable reduction of ductility.
- Fractography reveals the mechanisms of crack initiation and propagation that indicate transition from ductile to ductile-brittle cracking.

**Abstract:** The carbonized elastomer-based composites (CECs) possess a number of attractive features in terms of thermomechanical and electromechanical performance, durability in aggressive media and facile net-shape formability, but their relatively low ductility and strength limit their suitability for structural engineering applications. Prospective applications such as structural elements of MEMS can be envisaged, since smaller principal dimensions reduce the susceptibility of components to residual stress accumulation during carbonization, and to brittle fracture in general. We report the results of *operando* in-SEM study of micro-deformation and fracture behavior of CECs based on NBR elastomeric matrices filled with carbon and silicon carbide. Nanostructured carbon composite materials were manufactured via compounding of elastomeric substance with carbon and SiC fillers using mixing rolling mill, vulcanization, and low-temperature carbonization. Double Edge Notched Tensile (*DENT*) specimens of vulcanized and carbonized elastomeric composites were subjected to *in situ* tensile testing in the chamber of the scanning electron microscope (SEM) Tescan Vega 3 using Deben Microtest 1 kN Tensile Stage. The series of acquired SEM images were analyzed by means of Digital Image Correlation (DIC) using *Ncorr* open source software to map the spatial distribution of strain. These maps were correlated with Finite Element Modelling (FEM) simulations to refine the values of elastic moduli. Besides, the elastic moduli were derived from unloading curve nanoindentation hardness measurements carried out using NanoScan-4D tester and interpreted using the Oliver-Pharr method. Carbonization causes significant increase of elastic moduli from 0.86 ± 0.07 to 14.12 ± 1.20 GPa for the composite with graphite and carbon black fillers. Nanoindentation measurements yield somewhat lower values, namely, 0.25 ± 0.02 GPa and 9.83 ± 1.10 GPa before and after carbonization respectively. The analysis of fractography images suggests that crack initiation, growth and propagation may occur both at the notch stress concentrator and relatively far from the notch. Possible causes of such response are discussed, namely, (1) residual stresses introduced by processing; (2) shape and size of fillers; and (3) the emanation and accumulation of gases in composites during carbonization.

**Keywords:** composite materials; carbonized elastomeric matrices; C/SiC fillers; μ-DENT; *in situ* tensile test; Deben Microtest; Tescan Vega 3; NanoScan-4D; Digital Image Correlation (DIC).

 doi:10.20944/preprints202012.0276.v1

## 1. Introduction

The formulation and use of carbonized elastomer-based composites (CECs) developed in the last decade due to the attractive perspective of reasonable cost net-shaped fabrication of carbon components for oil mining submersible pumps, brakes, current collectors, and other applications [1]. High thermomechanical and electromechanical performance, and durability in aggressive media of these materials are, however, accompanied by limited ductility that is closely related with the porosity resulting from gas emanation during carbonization.

Brittleness reduces the suitability of CECs for structural engineering applications, promoting the search for functional applications, where mechanical performance does not represent the primary criterion. Hybridization or miniaturization of structural components seem to represent solutions where CECs can maximize the advantages of their performance.

Fuel cell applications offer a good example of a functional application where CECs can offer overall benefit. Significant progress has been made in the development and implementation of one of the types of fuel cells, namely, redox batteries with an electrolyte based on vanadium salts.

The principle of operation of a fuel cell is to convert chemical energy into electrical without combustion and the accompanying damage to the environment. Their inherent advantages are high efficiency and power density, durability, and low maintenance cost [2,3]. There are several main types of fuel cells, such as polymer electrolyte membrane fuel cells (PEMFCs), High-Temperature Polymer Electrolyte Membrane Fuel Cells (HTPEM FCs), Solid Oxide Fuel Cells (SOFCs) and Alkaline Membrane Fuel Cells (AMFCs), etc. Within this list, PEMFCs are considered to be most promising for research due to their high efficiency [4].

The primary materials for PEMFCs and HTPEM FCs are polybenzimidazole (PBI) [5,6], poly(arylene ether sulfone)s (PAES)s [7], poly(arylene thioether)s (PAT)s [8], poly(arylene ether ketone)s (PAEK)s [9], etc. Working in a temperature range of 160 to 180 °C, these materials have shown their best performance with power density values reaching 780 mW/cm$^2$.

The efficient operation of the membrane-electrode blocks requires high chemical and electrochemical resistance in combination with high electrical and thermal conductivity. Currently, fine-grained graphite and graphite-filled polymer compositions are widely used for these purposes. Artificial graphite has high chemical resistance and high electrical conductivity, minimizing electrical losses inside the block, whilst high thermal conductivity ensures heat dissipation and excludes local overheating inside the unit. Along with advantages, these systems have a severe disadvantage – electrochemical corrosion caused by the oxidation of boundaries between crystallites. The oxidation process has a significant effect on the durability of such blocks. Polymer-graphite compositions show high resistance to chemical and electrochemical corrosion, but unfortunately, they do not have high thermal and electrical conductivity. Another drawback of such materials is the heterogeneity of the structure caused by the difficulty to introduce large amount of conductive fillers and to ensure their homogeneous distribution. To obtain high thermal conductivity and electrical conductivity, it is necessary to reach high filling fractions, which dramatically reduces the strength and deformation characteristics of such materials.

Recently we put forward a paradigm for the promising alternative to PEMFCs, namely, carbonized elastomer-based composites (CECs), the conductive composite materials based on elastomeric matrices filled with various carbon fillers (carbon fibers, graphite, carbon black, shungite, carbon nanotubes and graphene) passed low-temperature carbonization. The technological workflow developed for CECs makes it possible to create highly filled structures containing up to 75 wt. % filler with highly uniform distribution in the elastomeric matrix [10,11]. Simultaneous use of different carbon fillers facilitates the creation of hierarchically structured heat-resistant material with good electrical conductivity.

The use of specific elastomers (NBR, HNBR, fluorinated caoutchouc) as primary composite matrices plays a vital role in forming composite materials resistant to aggressive media such as those used in fuel cells. The introduction of fillers into the elastomer matrix is carried out using proven rubber industry technologies that ensure uniform distribution of filler particles within the matrix.

Preprints (www.preprints.org) | NOT PEER-REVIEWED | Posted: 11 December 2020 doi:10.20944/preprints202012.0276.v1

Vulcanization at 160…180 °C yields complex net-shaped articles of high dimensional accuracy. Subsequent low-temperature carbonization at temperatures 320…360 °C significantly improves the elastic modulus and strength of the composite. It has been shown that fabricated CECs have high values of tensile, compressive, and flexural strength compared to well-known thermoplastic-based composites with polysulfone (PSU), polyphenylene sulfide (PPS), or polyetheretherketone (PEEK) matrices [10,11].

Due to the unavoidable release of gases (oxygen, hydrogen, nitrogen, and water vapor) in the core of composite, the internal porosity is formed. As a result, carbonized composites become brittle, and their elongation at fracture does not exceed 0.4 %. However, brittleness does not represent an insurmountable barrier for successful application when miniature articles are considered, since smaller principal dimensions and thinner cross-sections are less susceptible to residual stress accumulation during carbonization, and to brittle fracture, due to smaller volume for strain energy accumulation. Relatively weakly loaded membrane-electrode blocks in fuel cells and structural elements of MEMS are envisaged as prospective applications where brittleness of CECs may be tolerated. Thorough the characterization of micro-deformation and fracture behavior of CECs and the effect of carbonization is required to optimize the mechanical performance and to allow eventual formulation of predictive models for CAD purposes.

The present study addresses the details of the fracture mechanism in CEC materials subjected to tension. Special experimental setup was employed for *operando* in-SEM visualization and mapping of the spatial distribution and localization of strain in the vicinity of stress concentrators in DENT specimens. The strains determined using Digital Image Correlation (DIC) were correlated with the predictions of Finite Element Modelling (FEM) analysis to refine the values of elastic moduli. The values were compared with the data for elastic moduli obtained using Oliver-Pharr analysis of nanoindentation tests. The analysis of fracture surface appearance (fractography) was used to identify the mechanisms of crack initiation, growth and propagation at different extension rates.

## 2. Materials and Methods

### *2.1. Composite Sample Preparation*

CECs were prepared from three elastomeric compounds (of compositions given in Table 1) which were formulated and obtained to reach 300 phr filling degree (yielding therefore 75 m. %) through the filling of nitrile butadiene NBR caoutchouc matrix (JSC Krasnoyarsk SyntheticRubber Plant, Krasnoyarsk, Russia) with three types of carbon fillers: fine granular graphite (GMZ, Russia), dispersed carbon black (CB, N-399, Russia) and chopped carbon fibers (CFs, UKN-5000, Russia). SiC powder (64C, Russia) filler was also applied as a filler for comparison.

**Table 1.** Investigated compositions with labels.

| | **Graphite, phr** | **Carbon black, phr** | **Carbon fibers, phr** | **SiC, phr** |
|---|---|---|---|---|
| EC-FC-1 | 250 | 50 | – | – |
| EC-FC-2 | 225 | 50 | 25 | – |
| SiC | – | – | – | 300 |

CEC samples production was conducted in three stages. At the first stage, a crude elastomeric compound is obtained via mixing of caoutchouc and solid fillers using rubber mixing laboratory rolling mill (BL-6175-A, China). The second stage was the vulcanization of compounds at 170 °C and 5 MPa pressure during 10 min with the help of thermal press (AVPM-901, Russia). Vulcanization causes the spatial crosslinking in the compound matrix that results in the increase of its strength and elasticity accompanied by some decrease of plasticity. Composite samples assume their final shape at the vulcanization stage, when the rubber compound is pressed into individual purposefully designed molds. The final stage was the carbonization in a muffle furnace (PM-16M, Russia) at maximum temperature of 340 °C, which brings the properties CECs to the final values in a series of simultaneous thermal-oxidative destruction and secondary radical polymerization reactions. The workflow of preparation method is illustrated in Figure 1.

Preprints (www.preprints.org) | NOT PEER-REVIEWED | Posted: 11 December 2020 doi:10.20944/preprints202012.0276.v1

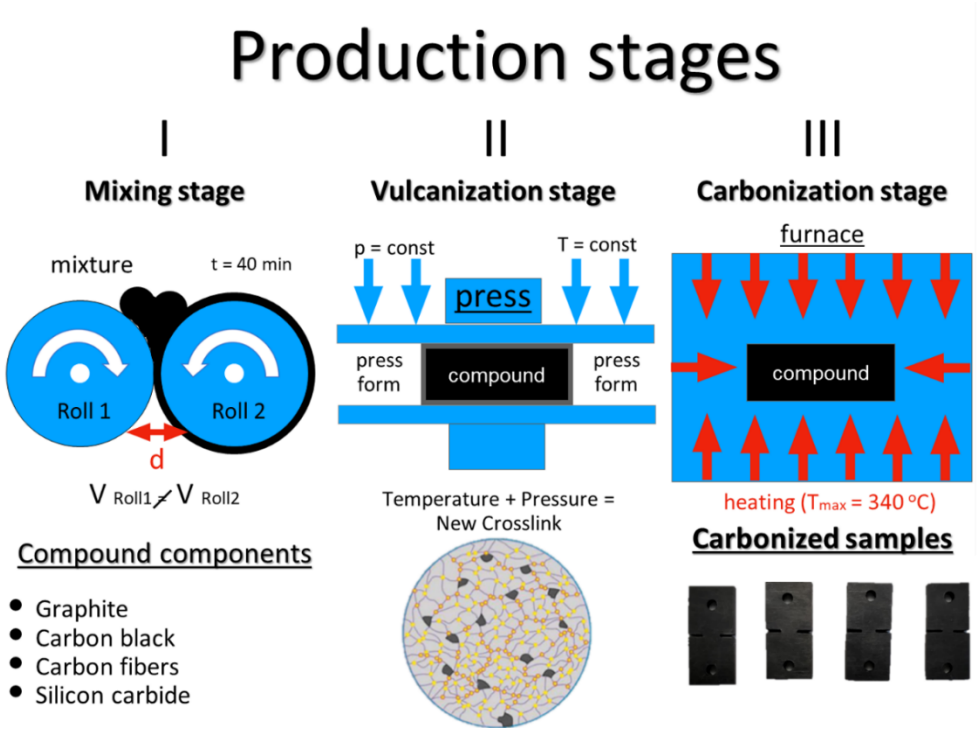


**Figure 1.** The workflow of preparation composite materials based on the carbonized polymer matrix.

Three samples of each compound composition were cut from the 3…4 mm thick rubber plates and tested after vulcanization and carbonization stages separately. CEC samples with DENT geometry were templated and further cut mechanically with a sharp knife. Polylactide (PLA) templates were additively manufactured using 3D printer Ultimaker 2+ (Ultimaker B.V., Utrecht, Netherlands). The shape and dimensions of CEC samples are shown in Figure 2. The latter were used in Deben Microtest 1 kN Tensile Stage (Deben UK Ltd., UK) in accordance with the requirements of ASTM E1820-11 [12] test standard.

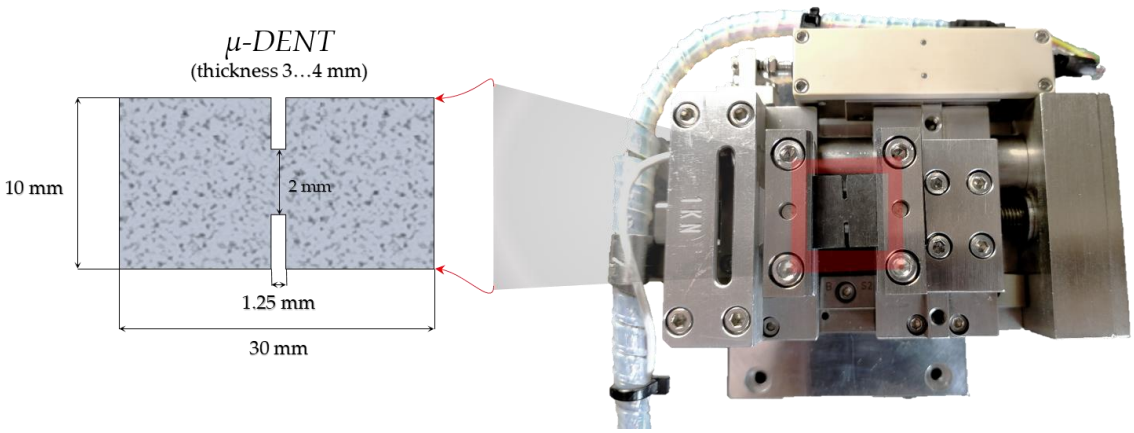


**Figure 2.** The shape and dimensions of *DENT* specimens.

Micro-deformation and fracture behavior of CECs after vulcanization and carbonization was studied using Deben miniature testing device in the chamber of SEM in tensile mode, and separately using NanoScan-4D hardness tester. The acquired SEM images were processed to compare the results of DIC analysis with FEA simulations. In addition, microstructure of fracture surfaces was observed to perform fractography analysis.

Preprints (www.preprints.org) | NOT PEER-REVIEWED | Posted: 11 December 2020 doi:10.20944/preprints202012.0276.v1

*2.2. In-SEM Operando Tensile Testing*

The tensile test was carried out *operando* in the chamber of a SEM Tescan Vega 3 (Tescan Company, Brno, Czech Republic) using Deben Microtest 1 kN Tensile Stage. Testing was conducted at permanent crosshead speed of 0.2 mm/min for the specimens of all compounds. Crosshead speed was varied (0.2, 0.5, 1.0, 1.5, and 2.0 mm/min) for the samples of carbonized SiC-filled composite to study the impact of tension rate on the elastic and fracture response. The experimental setup is illustrated in Figure 3.

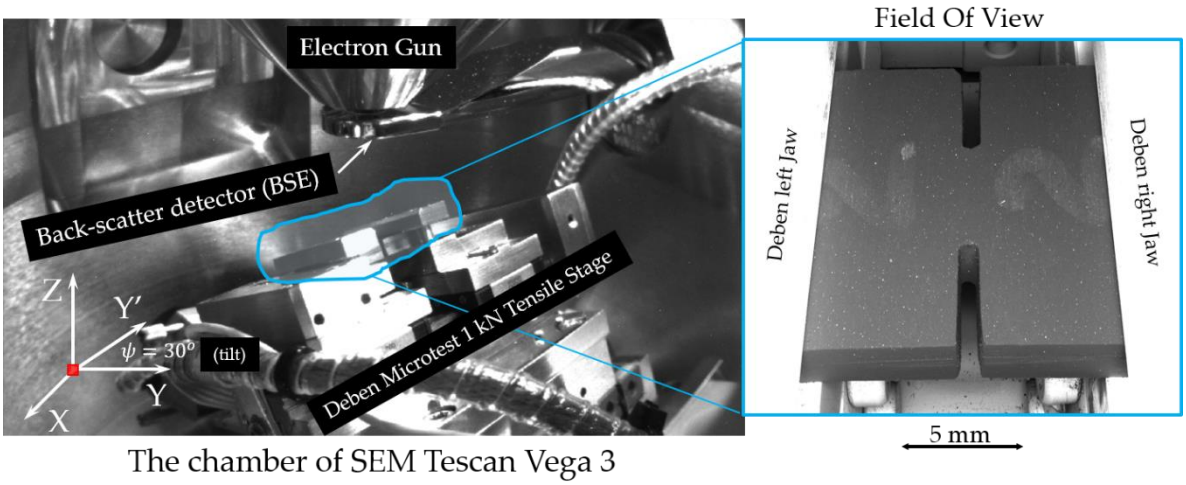


**Figure 3.** The view of the experimental setup – the chamber of the SEM Tescan Vega 3.

Deben Microtest 1 kN Tensile Stage was operated using bespoke Python code to synchronize the mechanical loading with the acquisition of SEM images. The acquisition rate of SEM images was 4 seconds per image (1 μs/pixel) using BSE regime with beam intensity of 15.00, beam size of 500.0 nm, depth of focus of 2.676 mm, working distance of 32.454 mm, chamber vacuum of 0.98 mPa, and column pressure of 0.25 mPa. Specimens were tested at 0° and 30° tilt position, with the latter used to detect cracks at both the upper and side surfaces.

Figure 4 presents the typical load-displacement curves recorded during tensile tests, along with the appearance of samples after fracture for CEC after vulcanization and carbonization, respectively.

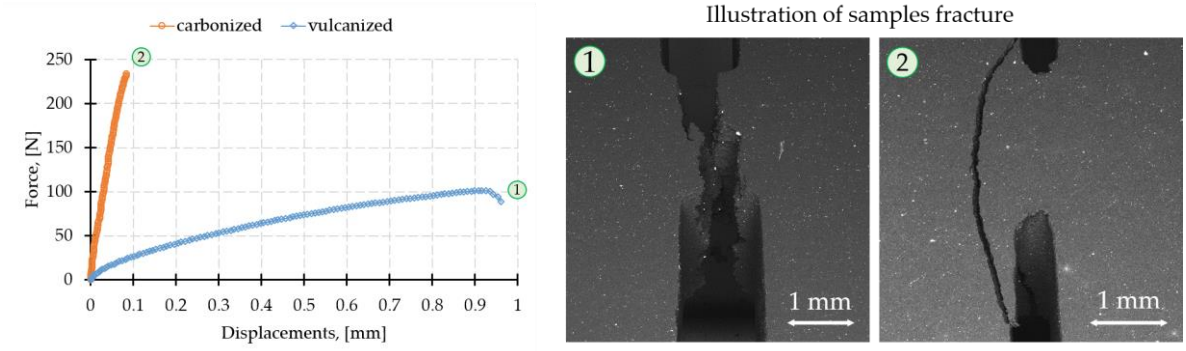


**Figure 4.** The typical load-displacement curves and fracture appearance for a CEC after vulcanization (1) and carbonization (2).

*2.3. Digital Image Correlation (DIC) and Finite Element Analysis (FEA)*

Digital Image Correlation (DIC) allows obtaining displacement and strain distributions for deforming specimens with subpixel resolution. Popular Matlab-based open-source software *Ncorr* that proved its versatility and robustness [13] was utilized for DIC analysis. The DIC algorithm is based on the finding of the best match between a chosen pixel subset of two states with the further conversion of determined pixel subset center positions to the displacement and ultimately to strains.

Preprints (www.preprints.org) | NOT PEER-REVIEWED | Posted: 11 December 2020 doi:10.20944/preprints202012.0276.v1

*Ncorr* code allows defining the regions of interest and applying various parameters such as shape, density of points, etc. to create correlation subsets, and eventually interpolating the results to form displacement and strain field maps. The pattern quality (the presence and density of surface features) of an image are crucial for the robustness of DIC analysis. There are several methods to improve the pattern quality, with paint sputtering being the most known and simple. In this paper, the particles of fillers were used as markers for the DIC analysis, as illustrated in Figure 5. The results of DIC analysis are exemplified in Figure 6.

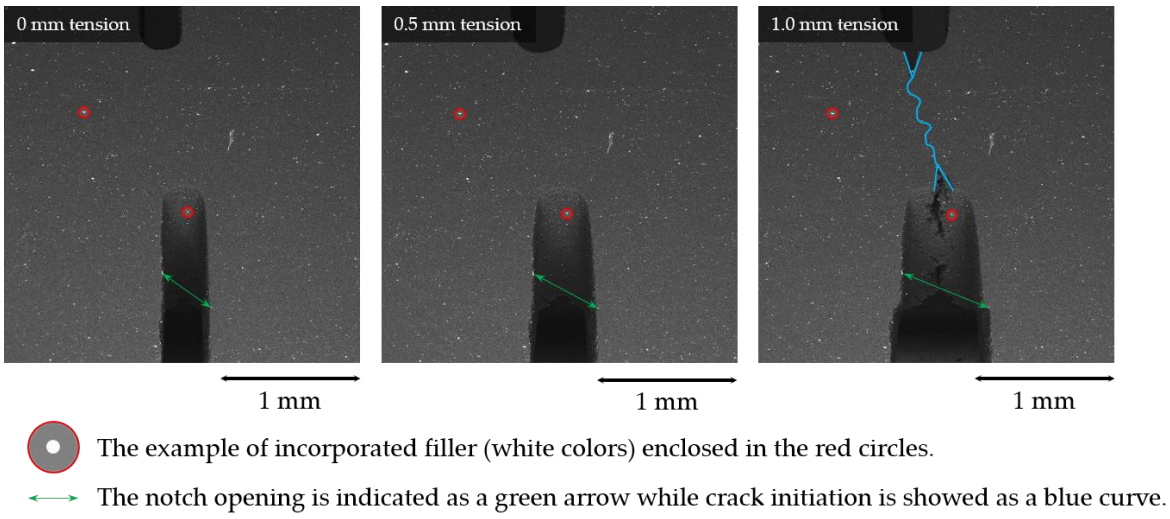


**Figure 5.** The pattern quality of the captured SEM images.

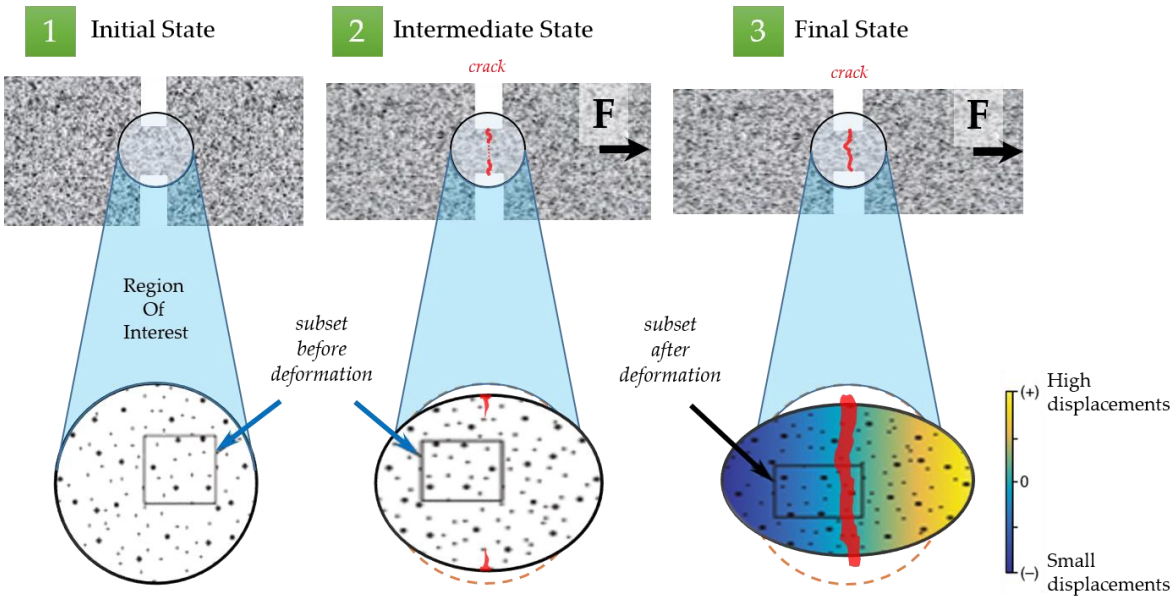


**Figure 6.** The workflow of the DIC analysis.

Since the distribution of displacements and strains is intrinsically inhomogeneous in the specimens with DENT concentrators, it was not possible to determine directly the elastic characteristics such as Young's modulus and Poisson's ratio. For this purpose, FEA of DENT specimens was performed using Autodesk Fusion 360 [14], with the constraints and force application as indicated in Figure 7.

Preprints (www.preprints.org) | NOT PEER-REVIEWED | Posted: 11 December 2020 doi:10.20944/preprints202012.0276.v1

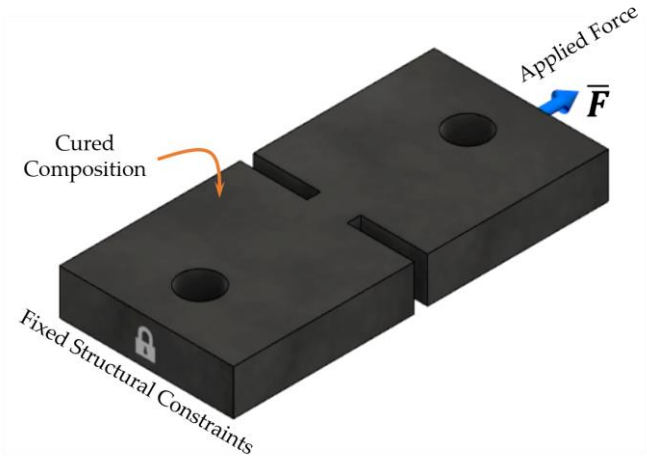


**Figure 7.** The schematic for FEA simulation.

*2.4. Fractography Analysis*

Fractography is a well-known approach to deduce the underlying physical mechanisms of fracture and to characterize the crack propagation processes via the examination of fracture surface images acquired using different techniques such as SE or optical microscopy[15]. Ductile fracture evolves through the creaton of microvoids desintegrating the material at the fracture surface, then their growth and coalescence to larger voids accompanied with intense plastic flow result in the ultimate destruction. Brittle farcture suggests the development of cracks along weak interior interfaces or weak thin bands within a phase. Fracture surfaces were studied using SEM Tescan Vega 3 at various magnifications. The examples of fracture surface images used for fractography analysis are represented in Figure 8.

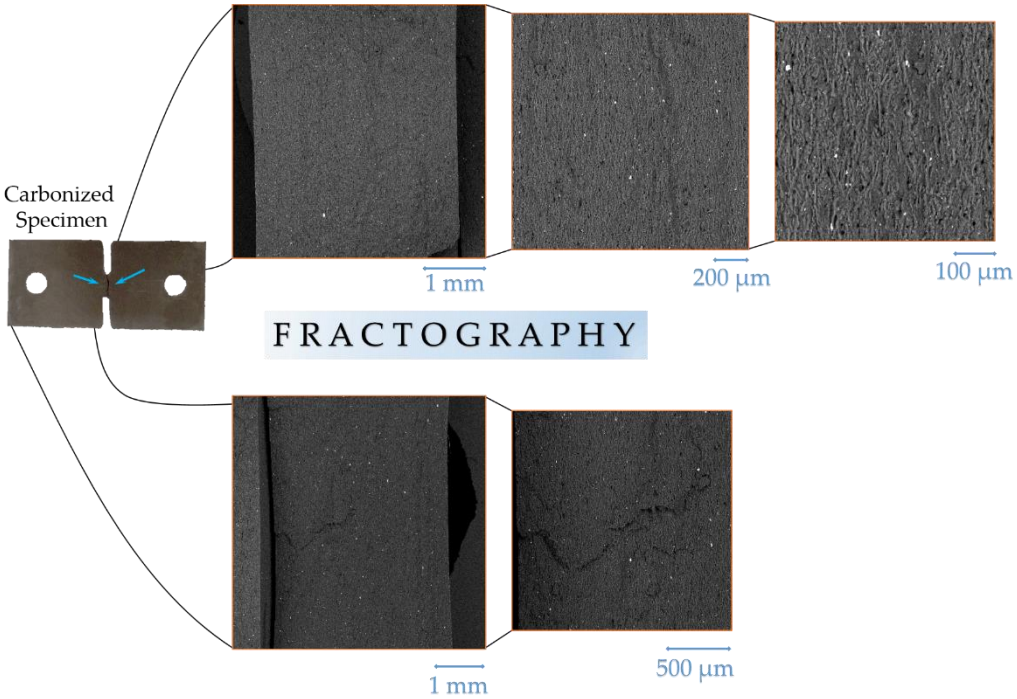


**Figure 8.** An example of fractography analysis in CEC specimens.

*2.5. Nanoindentation Analysis*

The nanoindentation tests were carried out at ambient temperature using a scanning nano-hardness NanoScan-4D tester (NanoScan Company, Troitsk, Russia) equipped with diamond

Preprints (www.preprints.org) | NOT PEER-REVIEWED | Posted: 11 December 2020 doi:10.20944/preprints202012.0276.v1

Berkovitch pyramid. The samples of CECs after vulcanization and carbonization stages were serially indented along a 10 mm line with 250 μm step between individual indents. A linear force increment mode was applied: maximum force was set as 1 N, the load time of 1 s, the hold time of 0.5 s, and free unloading time. Typical indentation curves are demonstrated in Figure 9. Processing of "load-displacement" curves was conducted in accordance with Oliver-Pharr method [16] and ISO 14577 standard [17] to distract the estimates for Young's modulus and hardness.

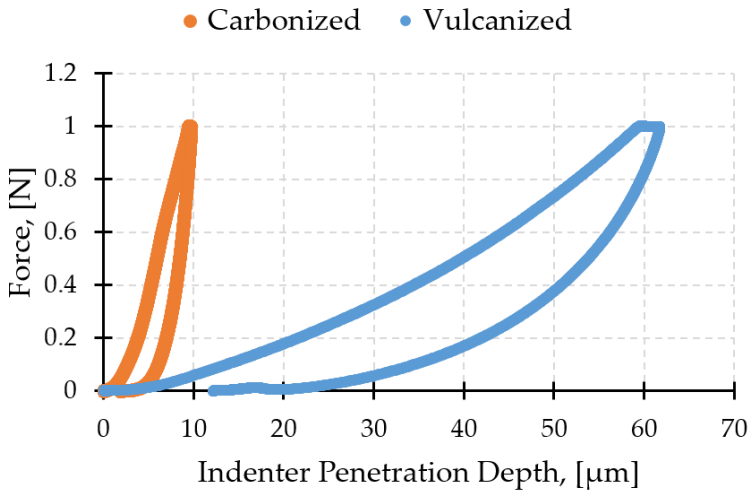


**Figure 9.** Typical load-displacement curve at nanoindentation.

## 3. Results and Discussion

### *3.1. Operando Tensile Testing*

Mechanical characteristics of CECs extracted from stress-strain curves (Figure 10) are summarized in the Table 2. Taking into account the values of Young's modulus for filler particulates (10-25, 250-650 and 350-450 GPa for graphite, carbon fibers and SiC respectively) one can conclude that simple additive rule of mixture is not valid for elastic modulus and ultimate tensile strength of vulcanized CECs assuming that matrix-filler bonding is likely to be predominant factor governing their elastic and plastic behavior.

**Table 2.** Mechanical properties of CECs.

| Composite | | Elastic modulus, GPa | Ultimate Tensile Strength, MPa | Elongation at Break |
|---|---|---|---|---|
| EC-FC-1 | Vulc. | 0.86 ± 0.07 | 9.80 | 0.029 |
| | Carb. | 14.12 ± 1.20 | 29.22 | 0.0028 |
| EC-FC-2 | Vulc. | 0.44 ± 0.05 | 9.50 | 0.040 |
| | Carb. | 7.85 ± 1.51 | 11.75 | 0.0022 |
| SiC | Vulc. | 0.098 ± 0.006 | 4.07 | 0.126 |
| | Carb. | 13.60 ± 1.34 | 23.14 | 0.0026 |

On the other hand, vulcanized CECs having been purposefully developed as the particulate reinforced composites of very high filling degree (75 %) may reveal ductile (EC-FC-1 and SiC) or brittle character (EC-FC-1) of fracture depending on the nature of fillers. It seems that quasi-uniaxial particulates in EC-FC-1 and SiC promote some ductility while sharp long fibers are likely to introduce internal concentrators facilitating easy crack propagation.

Carbonization at temperatures below 500 °C involves diverse processes unfolding at heating: dewatering, emanation of volatile light hydrocarbon fractions, oxidative dehydropolycondensation, thermodectruction in side and further in main chains to form radicals, polymerization of radicals, and, therefore, introduces numerous defects and imperfections at nanometer, supramolecular

Preprints (www.preprints.org) | NOT PEER-REVIEWED | Posted: 11 December 2020 doi:10.20944/preprints202012.0276.v1

dimensional level. Gradual emanation of gases creates pores of submicron and micrometer size frequently associated with filler particulates that weakens the effect of reinforcement. Thermal gradients occurring in big cross-sections at relatively high heating or cooling rates may additionally introduce residual stresses affecting the strength of CEC parts at millimeter dimensional level. The interaction of hierarchically different phenomena takes place in real CEC products such as fuel cell membrane-electrode blocks.

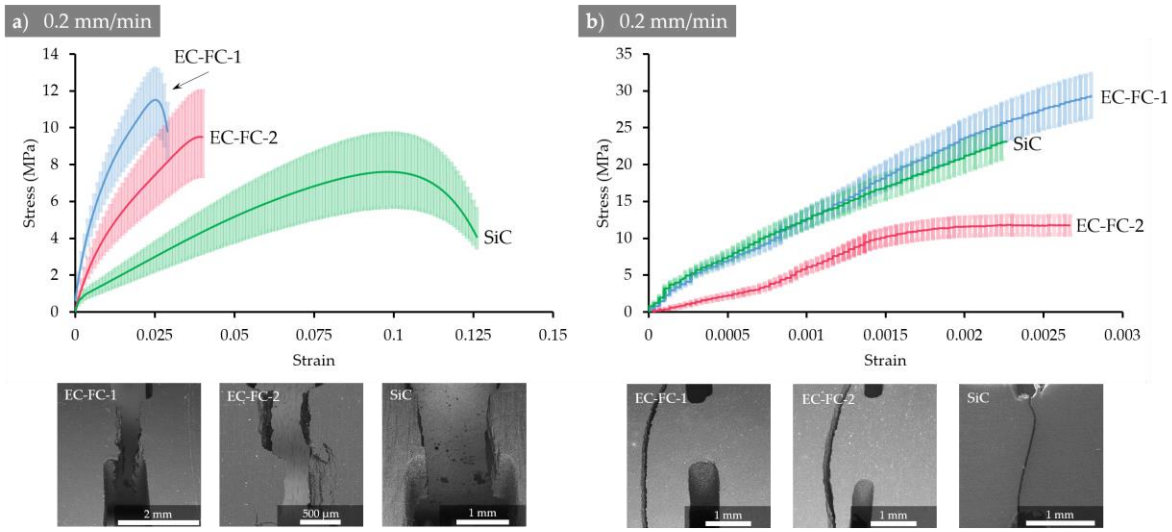


**Figure 10.** Experimental stress-strain curves with indicated 95 % confidence interval for (**a**) vulcanized and (**b**) carbonized specimens that were tested at constant crosshead speed of 0.2 mm/min. The appearance of broken samples is shown in the lower row of images.

As it can be concluded from the data represented in Table 2 and Figure 10 carbonization significantly improves elastic modulus (at for one order of magnitude) and almost doubles ultimate tensile strength for EC-FC-1 and SiC composites. The elongation at break is, however, at least for 10 times smaller in carbonized CECs samples with DENT concentrators in comparison with vulcanized counterparts making former ones purely brittle. It is worth noting that crack may pass away from the concentrator, what may suggest: a) the distortion of stress field pattern from the anticipated one due to the presence of residual stresses; b) the presence of hidden defects.

This observation is additionally supported by the results obtained for carbonized SiC-filled CEC samples at crosshead speed 0.5; 1.0; 2.0; 1.5 mm/min (Figure 11). Ultimate tensile strength significantly varies in the range of 4.48 … 26.57 MPa showing no clear dependence on crosshead speed, while elongation at break is much less variable and apparently independent on crosshead speed. The crack may be localized in the DENT neck (1.0 and 2.0 mm/min) or may pass away from the concentrator. This random character of micro-deformation and fracture behaviour pursues to conclude that inhomogeneity of material properties (local flaws or pores and superposition of tensile residual stress) is the key issue to be mitigated in further technological developments.

Preprints (www.preprints.org) | NOT PEER-REVIEWED | Posted: 11 December 2020 doi:10.20944/preprints202012.0276.v1

SiC carbonized specimens

| Traverse Speed, mm/min | Fracture Strength, MPa | Elongation of Break |
|---|---|---|
| 0.5 | 4.48 | 0.0025 |
| 1.0 | 25.08 | 0.0032 |
| 1.5 | 26.57 | 0.0024 |
| 2.0 | 19.27 | 0.0020 |

**Figure 11.** Experimental characteristics obtained for carbonized specimens filled with SiC and tested for 0.5, 1.0, 1.5, and 2.0 mm/min traverse speeds.

*3.2. Fractography Analysis*

Macroscopic appearance of fracture surfaces in various prospective is given in Figure 12 for vulcanized and carbonized composites. It can be seen that in contrast to vulcanized samples which always fracture across the DENT concentrator neck, some carbonized samples show a complex crack propagation paths involving broad zones away from the concentrator and shortest path across the DENT concentrator neck.

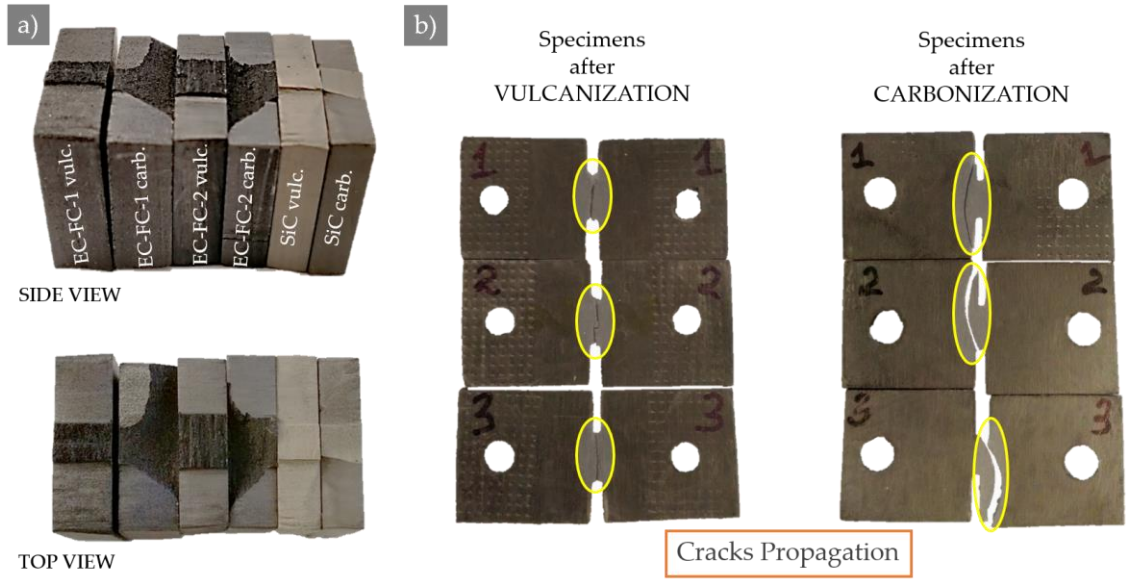


**Figure 12.** The example of macro view for different specimens in various prospective.

The structure of crack surfaces as seen in Figure 13 depends on the nature of filler. The crack surface of SiC-filled composite contains many elliptic microscopic hollows. Thus, tensile fracture mechanism in this composite corresponds mainly to the pull-out of reinforcing particulates from the matrix. A number of microcracks in combination with round hollows were observed at the fracture surface of EC-FC-2 composite samples. The crack surfaces of EC-FC-1 samples reveal no pores, holes or microcracks that correlates with the best mechanical performance in the series of CEC samples studied.

Preprints (www.preprints.org) | NOT PEER-REVIEWED | Posted: 11 December 2020 doi:10.20944/preprints202012.0276.v1

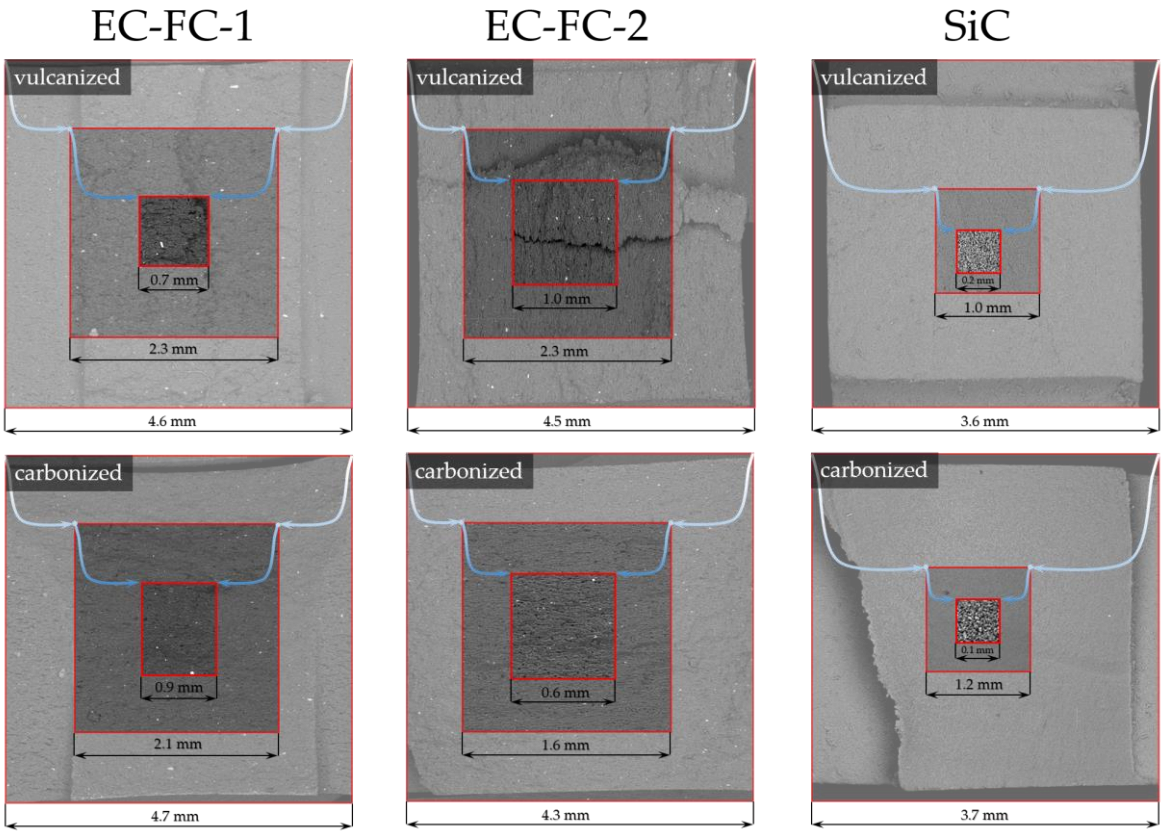


**Figure 13.** The microscopic appearance of sample fracture surfaces.

*3.3. Correlation of DIC and FE Analysis*

The correlation of DIC and FE analysis results was carried out for vulcanized EC-FC-1 composite only since: 1) this composite has highest mechanical performance after carbonization; 2) cracking develops too fast in carbonized composites that makes impossible to capture sufficient number of SEM images (each requires at least 4 seconds) and to reach satisfactory quality of SEM images for reliable DIC analysis.

The pattern of experimentally DIC-detected along X-axis displacements and strains in the vicinity of DENT concentrator is demonstrated in Figure 14 for several points at stress-strain curve obtained from Deben Microtest device. The nominal stress was calculated as the force per cross-sectional area of the ligament, while strain was found as ratio of sample elongation to the initial distance between device jaws. The pattern of displacements almost exactly corresponds to the predictions of classical fracture mechanics theory, i.e. under tension an elliptical region appears of rapid variation of the longitudinal displacement, with the major semi-axis parallel to loading direction. The strain distribution is clearly inhomogeneous, with the highest strain values present at the notch tips, and a central region of relatively low strains located in the middle of DENT neck. The strain field has a shape of a doughnut elongated parallel to the X axis and the transverse diameter approximately equal to the width of the DENT sample ligament.

Inhomogeneous strain distribution prevents direct calculation of elastic characteristics (Young's modulus and Poisson's ratio) from the data on load and strains as it can be easily carried out for un-notched samples. Therefore, a FE simulation of strain field in dimensionally identical model was performed and the patterns of strain fields were correlated (carefully calibrated) with the pattern of experimentally determined strains (Figure 15). Varying the values elastic characteristics and assuming that model isotropic material contains no pores, cracks or other defects it was found that the best correlation (match) of the modelled strain field with the experimental one is reached for Young's modulus of 1 GPa, Poisson's ratio of 0.40, ultimate tensile strength of 10 MPa and density of 1.61 g/cm$^3$. It is worth to note that the central spot of relatively low strains could not be reproduced

Preprints (www.preprints.org) | NOT PEER-REVIEWED | Posted: 11 December 2020 doi:10.20944/preprints202012.0276.v1

in simulations, however, the presence of star-shaped zones of relatively low strains in modelled samples is also detected in the middle of DENT neck.

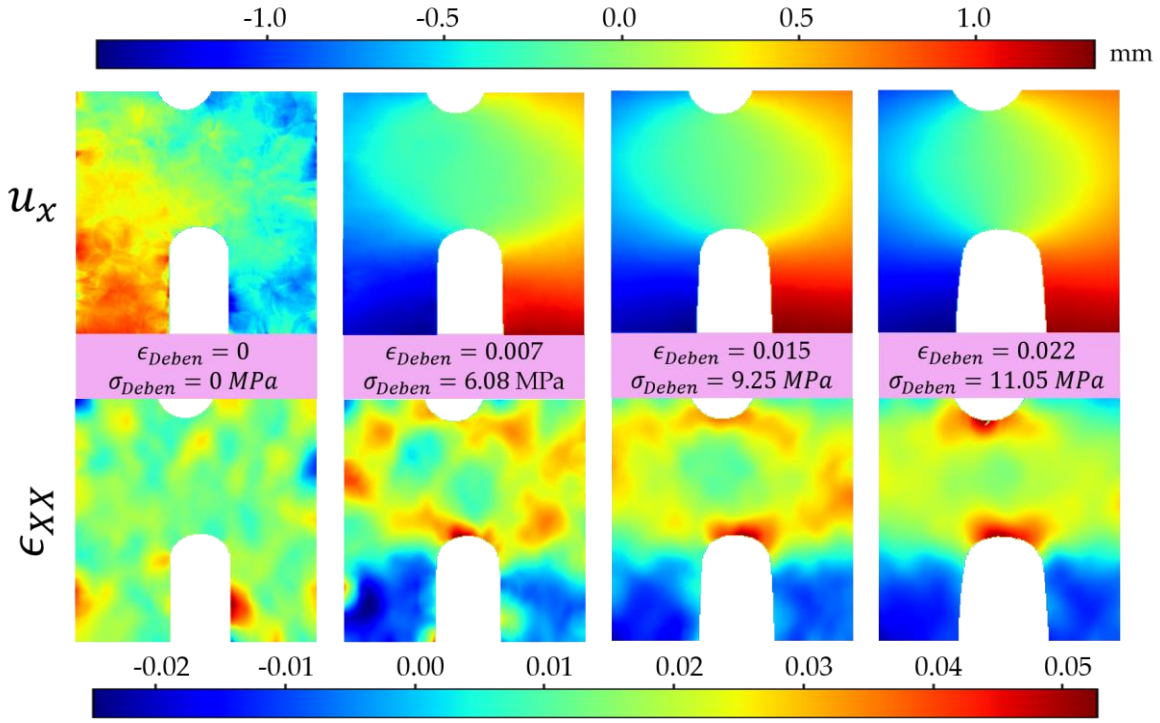


**Figure 14.** Displacement (**top**) and stain (**below**) distribution along X-axis at nominal macro strain values of 0, 0.007, 0.015 and 0.022, respectively.

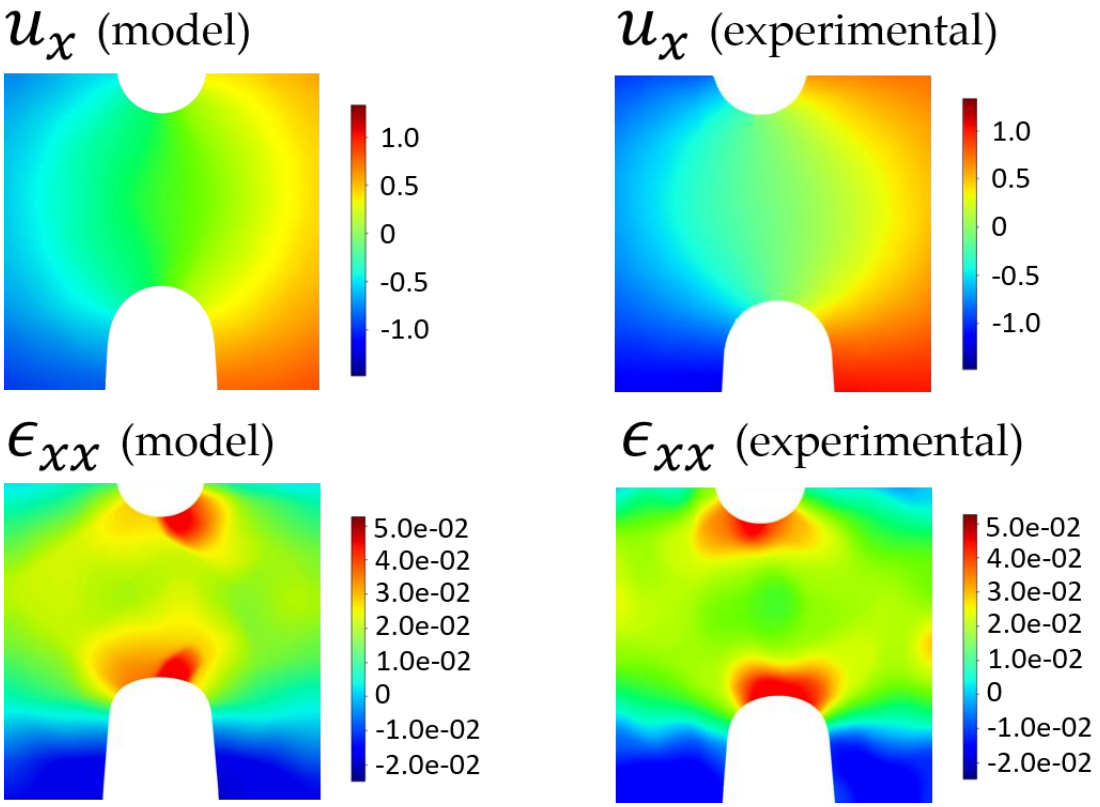


**Figure 15.** Correlation of modelled (**left**) and experimental (**right**) strain fields.

Preprints (www.preprints.org) | NOT PEER-REVIEWED | Posted: 11 December 2020 doi:10.20944/preprints202012.0276.v1

*3.4. Nanoindentation Test*

Roughness profiles of samples' surface was checked (Figure 16 and Figure A1) before nanoindentation tests to fulfill the requirements on the indentation depth that must be in accordance with the Section 2.5. of ISO 14577 standard at least 20 times bigger than Ra. Ra roughness at the surface of vulcanized and carbonized samples of EC-FC-1 composite is 0.54 ± 0.10 and 0.51 ± 0.07 μm, respectively. Thus, the indentation depth about 10 μm is a satisfactory value for reliable results.

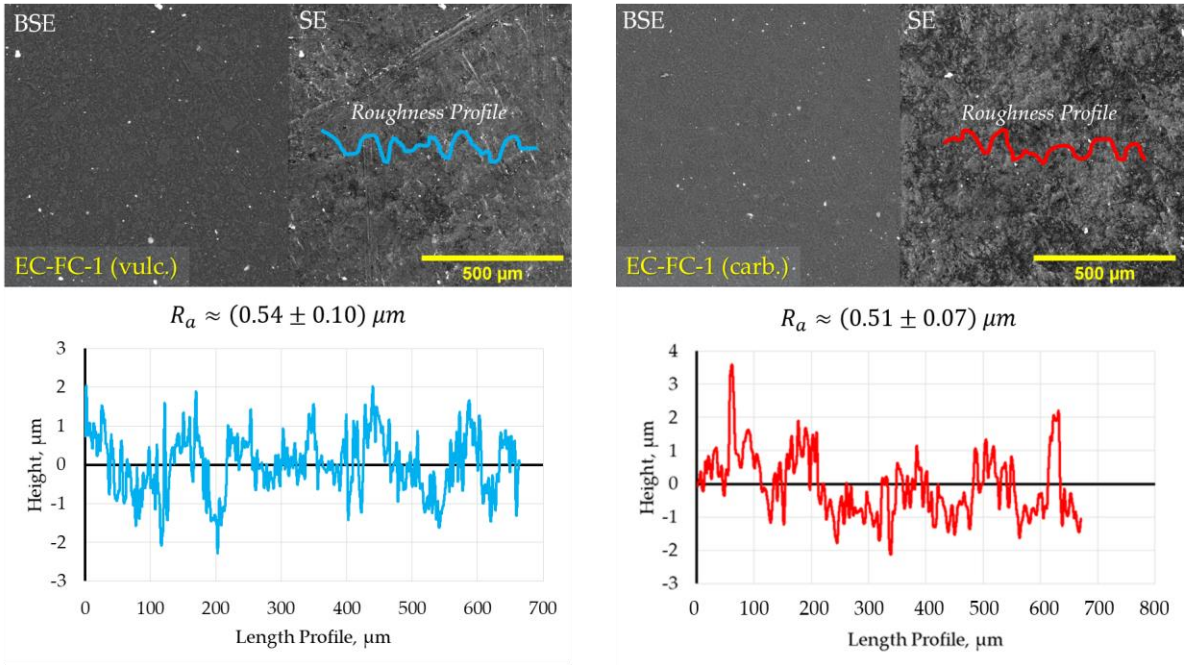


**Figure 16.** The roughness profile for vulcanized (**left**) and carbonized (**right**) specimens of EC-FC-1 composition.

The statistics of experimentally measure Young's modulus values for EC-FC-1 composite (Figure 17) returns the average value of 0.25 ± 0.02 GPa for vulcanized samples and 9.83 ± 1.10 GPa for carbonized samples, for the latter the values of Young's modulus occur to be quite close to the values of elastic modulus derived from tensile testing.

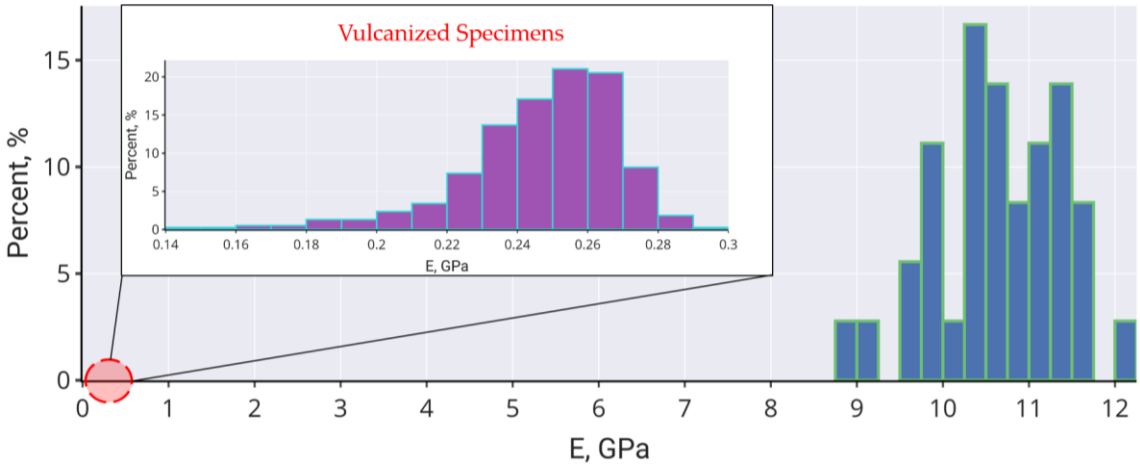


**Figure 17.** The Young's modulus distribution of vulcanized (**purple**) and carbonized (**blue**) specimens of EC-FC-1 composite.

 doi:10.20944/preprints202012.0276.v1

## 4. Conclusions

Carbonized elastomer-based composites reinforced by carbon and silicon carbide fillers can be easily net-shaped, they are durable in aggressive media, relatively strong but brittle, therefore, these composites are attractive for applications excluding significant mechanical loads or impacts. Membrane-electrode blocks in fuel cells and MEMS are viewed as perspective fields for CECs requiring, however, thorough characterization of micro-deformation and fracture behaviour. Double Edge Notched Tensile concentrators facilitate to limit the size of field of view for *operando* in-SEM tensile testing. This methodological approach was systematically implemented through the creation of dedicated experimental setup synchronizing Deben Microtest 1 kN Tensile Stage with scanning system of Tescan Vega 3 SEM. The specimens of CECs prepared using multistage technology that involved mixing, vulcanization, and carbonization stage were tested in tension in the chamber of SEM to acquire a series of high resolution SEM images for further DIC processing.

Patterns of inhomogeneous strain field are required to be correlated with the results of FE simulations (carried out using Autodesk Fusion 360 program in this research) in order to derive elastic characteristics. On the other hand, these characteristics are able to be calculated from nanoindentation force-displacement curves acquired using NanoScan-4D hardness tester. Fractography analysis of SEM images collected for fracture surfaces helps to highlight particular mechanisms and role of filler nature in crack initiation, growth and propagation.

CEC filled with graphite filler showed the best overall mechanical performance both in vulcanized and carbonized state – the highest values of elastic modulus and ultimate tensile strength in combination with acceptable and superior ductility in vulcanized and carbonized state respectively. Partial replacement of graphite particulates by carbon fibers aggravate both rigidity, strength and ductility in carbonized state in comparison with the optimal composite. The effect of filling with SiC particulates is controversial in carbonized state – high strength and low ductility. Nanoindentation testing returns somewhat smaller values of elastic characteristic that may reflect the impact of the defects/porosity/etc.

Cracks connect notch tips directly passing DENT neck along the shortest path in vulcanized composites. In contrast, in carbonized composites cracks can pass the samples along curved trajectories laying away from the DENT concentrator. This hints the presence and strong influence of residual stresses inherited after carbonization stage.

Preprints (www.preprints.org) | NOT PEER-REVIEWED | Posted: 11 December 2020 doi:10.20944/preprints202012.0276.v1

**Appendix A**

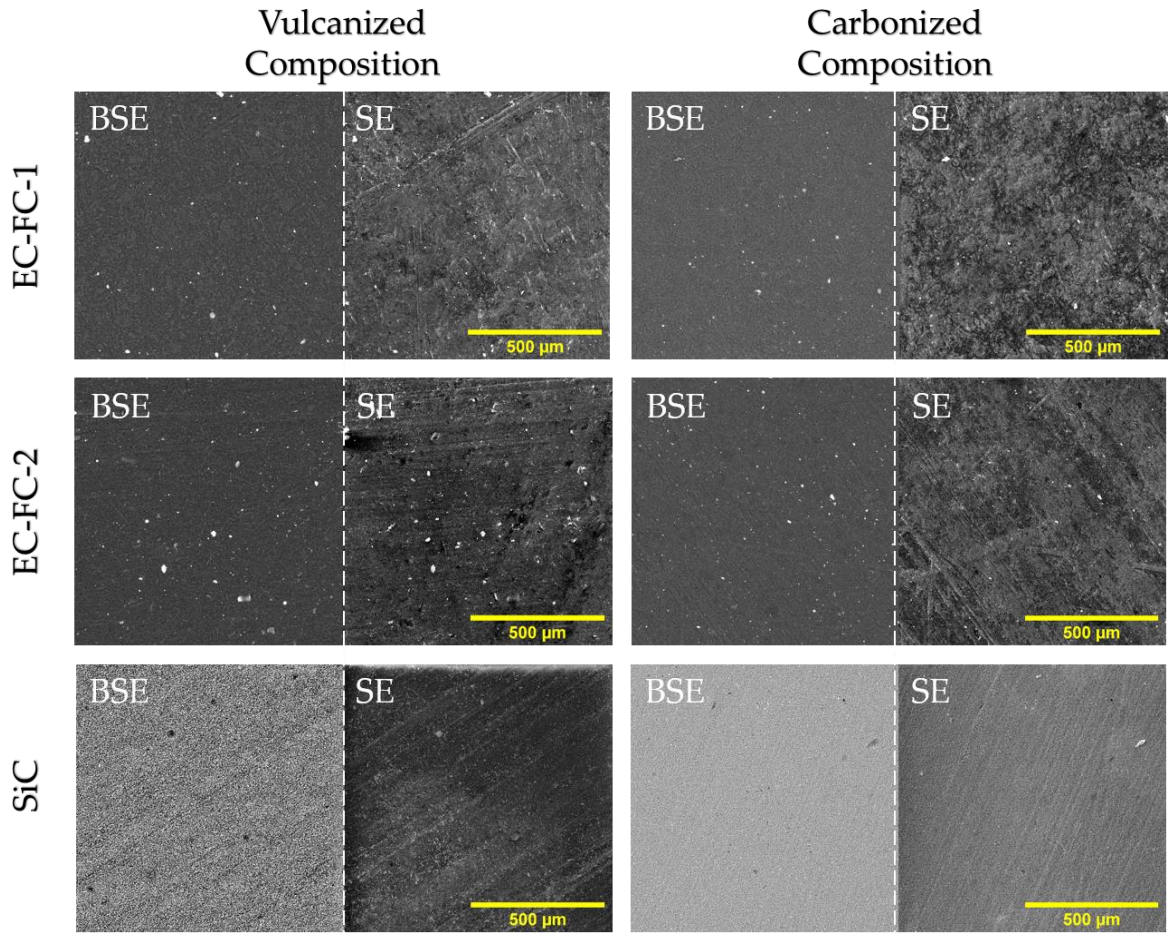


**Figure A1.** The microstructure of prepared samples with the different composition.

**Author Contributions:** Conceptualization, A.A.S., D.Ch., and S.D.K.; methodology, A.A.S, and S.D.I.; software, E.S.S., and A.I.S.; validation, A.A.S. and A.M.K.; formal analysis, E.S.S., and S.D.I..; investigation, E.S.S.; resources, E.S.S., and S.D.I.; data curation, E.S.S., and S.D.I.; writing—original draft preparation, E.S.S., S.D.I., A.I.S., and A.M.K.; writing—review and editing, A.S.S., D.Ch., and S.D.K.; visualization, E.S.S., and S.D.I.; supervision, S.D.K.; project administration, A.A.S.; funding acquisition, A.A.S. All authors have read and agreed to the published version of the manuscript.

**Funding:** This work was supported by the Ministry of Science and Higher Education of Russia in the frame of the state assignment, state program of basic research "For the long-term development and ensuring the competitiveness of society and the state" (47 GP) on the base of the universities, the plan of basic scientific research no. 718/20 dated 03/06/2020, project no. 0718-2020-0036.

**Conflicts of Interest:** The authors declare no conflict of interest.

**References**


1. Stepashkin A.A., *et al.* / Carbonised composite materials based on elastomers filled with carbon nanofillers // *Micro&Nano Letters*, **2018**, 13(5), 588.
2. M.K. Debe / Electrocatalyst approaches and challenges for automotive fuel cells // *Nature*, **2012**, 486, 43–51.
3. I.E.L. Stephens, J. Rossmeisl, I. Chorkendorff / Toward sustainable fuel cells // *Science*, **2016**, 354, 1378–1379.
4. G. Wanga, Y. Yub, H. Liua, Ch. Gonga, Sh. Wena, X. Wangc, Zh. Tud / Progress on design and development of polymer electrolyte membrane fuel cell systems for vehicle applications: a review / *Fuel Processing Technology*, **2018**, 179, 203–228.
5. N.N. Krishnan, A. Konovalova, D. Aili, Q. Li, H.S. Park, J.H. Jang, H.J. Kim, D. Henkensmeier / Thermally crosslinked sulfonated polybenzimidazole membranes and their performance in high temperature polymer electrolyte fuel cells // *J. Membr. Sci.*, **2019**, 588.
6. M.R. Berber, N. Nakashima / Bipyridine-based polybenzimidazole membranes with outstanding hydrogen fuel cell performance at high temperature and non-humidifying conditions // *J. Membr. Sci.*, **2019**, 591.
7. Y. Sui, Y. Du, H. Hu, J. Qian, X. Zhang / Do acidase interactions really improve the ion conduction in a proton exchange membrane? – a study on the effect of basic groups // *J. Mater. Chem.*, **2019**, 7.
8. C.Y. Wong, W.Y. Wong, K. Ramya, M. Khalid, K.S. Loh, W.R.W. Daud, K.L. Lim, R. Walvekar, A.A.H. Kadhum / Additives in proton exchange membranes for low- and high-temperature fuel cell applications: a review // *Int. J. Hydrogen Energy*, **2019**, 44.
9. J. Jang, D.H. Kim, M.K. Ahn, C.M. Min, S.B. Lee, J. Byun, C. Pak, J.S. Lee / Phosphoric acid doped triazole-containing cross- linked polymer electrolytes with enhanced stability for high-temperature proton exchange membrane fuel cells // *J. Membr. Sci.*, **2020**, 595.
10. D.I. Chukov, A.A. Stepashkin, A.I. Salimon, S.D. Kaloshkin / Highly filled elastomeric matrix composites: structure and property evolution at low temperature carbonization // *Materials and Design*, **2018**, 156, 22–31.
11. A.A. Stepashkin, D.I. Chukov, S.D. Kaloshkin, I.S. Pyatov, and M.Y. Deniev / Carbonized elastomer based composites filled with carbon fillers and silicon carbide // *Materials Letters*, **2018**, 215, 288–291.
12. ASTM E1820-11 [Electronic Resource]. Available online: www.astm.org (accessed on 6 November 2020).
13. Blaber J., Adair B., Antoniou A. / Ncorr: Open-source 2D Digital Image Correlation Matlab software // *Exp. Mech.* **2015**, 55, 1105–1122.
14. Autodesk Fusion 360 [Electronic Resource]. Available online: www.autodesk.com (accessed on 28 November 2020).
15. Fractography [Electronic Resource]. Available online: www.nanoscience.com/applications/materials-science/fractography/ (accessed on 28 November 2020).
16. Oliver W.C., Pharr G.M. / An improved technique for determining hardness and elastic modulus using load and displacement sensing indentation experiments // *J. Mater. Res.* **1992**, 7, 1564-1583.
17. ISO 14577 [Electronic Resource]. Available online: www.iso.org (accessed on 6 November 2020).